Supplementary Information for

Cell contraction induces long-ranged stress stiffening in the extracellular matrix.

By Yu Long Han, Pierre Ronceray, Guoqiang Xu, Andrea Malandrino, Roger Kamm, Martin Lenz, Chase P. Broedersz and Ming Guo

1 Experimental methods and supplementary experimental results.

1.1 Data analysis for active microrheology and measurements of collagen micromechanics

To manipulate a trapped bead, a high-resolution piezo stage is displaced at a constant velocity, v_{stage} = 1 μm/s. The distance between the laser and the bead is recorded using a quadrant photodiode detector (QPD) as a voltage signal, as shown by the black curve in Supplementary Figure 1a. This data is fitted with a quadratic function, $V(t)= at^2+bt$ (red curve), which is used in the following analysis to calculate the differential stiffness, k_{nl}. The voltage from the QPD is converted into the distance between the laser and the bead, D_{laser}, through a proportionality factor β, i.e. $D_{laser}(t)= \beta V(t)$, as shown by the black curve in Supplementary Figure 1b. The bead displacement relative to the stage is then calculated using $x(t)= v_{stage}*t- D_{laser}(t)$, as depicted by the red curve in Supplementary Figure 1b. The force on the bead is proportional to the distance between the laser and the bead, $F(t) = k*D_{laser}(t)$, where k is the trap stiffness.

The force-displacement relationship for a bead inside a collagen gel is then obtained as shown in Supplementary Figure 1c. The slope of this curve, which represents the effective stiffness of the gel, increases significantly as the applied force increases, suggesting a strong nonlinear stiffening effect in the collagen gel at the microscale. Indeed, the stiffness of the gel increases by two orders of magnitude as the applied force is increased, as indicated by the relationship between differential stiffness, k_{nl}, and applied force shown in Supplementary Figure 1d.

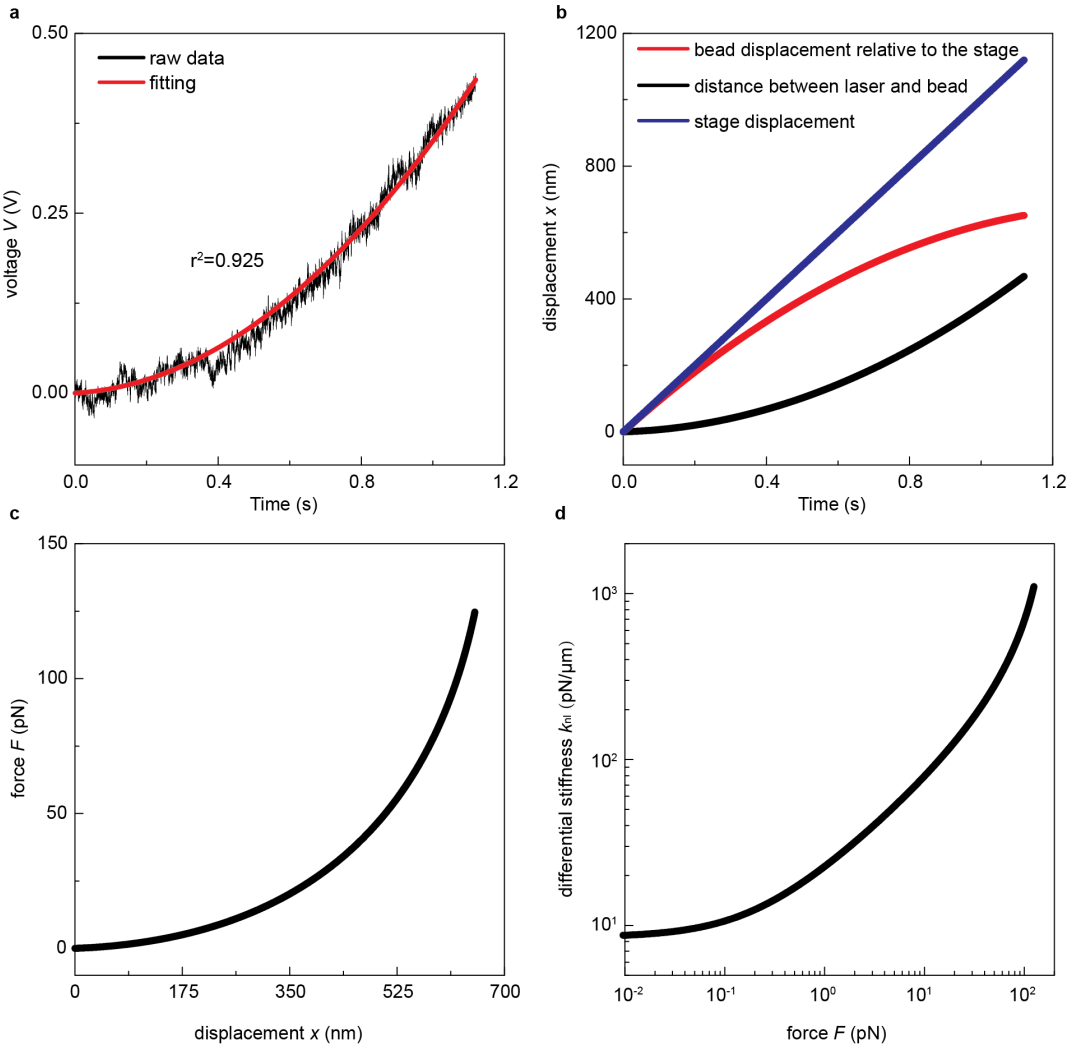

Supplementary Figure 1: Data analysis for active microrheology. **a**, Voltage reading from the quadrant photodiode detector (QPD) during mechanical testing, which reflects the relative position between laser trap and particle. The black curve shows the raw data, and the red curve shows the quadratic fit. **b**, Position information of laser, bead, and stage. Stage displacement stands for the displacement that the stage moves. **c**, The force-displacement curve obtained in 1.5 mg/mL collagen I sample far away from the cell. **d**, Force-differential stiffness curve obtained in 1.5 mg/mL collagen I sample far away from the cell.

1.2 Rate dependence and reversibility of micromechanical response

To investigate whether the mechanical response of the collagen matrix is rate dependent, we drag a 4.5-μm-diameter bead using optical tweezers to measure the force-displacement relationship at three different locations in a 1.5 mg/mL collagen I gel; at each location, we drag the bead three times with three different speeds, 0.5, 1, 1.5 μm/s, respectively, to measure the collagen micromechanics at different effective strain rates. We find that the resultant force-displacement

relationships obtained at varying speeds are very close to each other (Supplementary Figure 2a), suggesting that the micromechanics of the collagen matrix is rate-independent within the range of loading speeds in our study. Furthermore, we have also confirmed that the nonlinear force-displacement relationship measured in the collagen sample is fully reversible with negligible plastic effects, as similar force-displacement curves are obtained from repeated cyclic loading using the same bead, as shown in Supplementary Figure 2b.

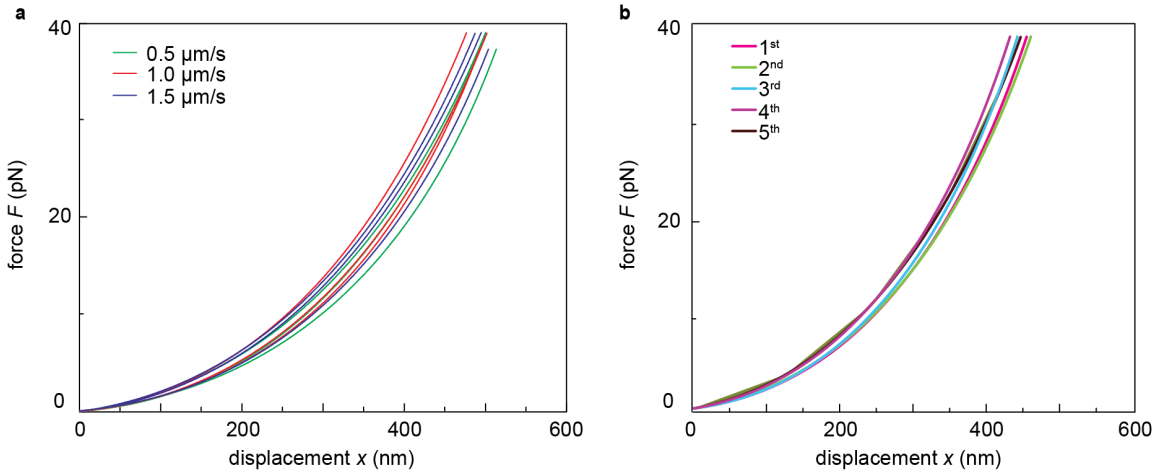

Supplementary Figure 2: Micromechanics of collagen matrix measured with optical tweezers. **a**, Force-displacement relationship measured using optical tweezers at different loading rates at 3 different locations in a 1.5 mg/mL collagen gel. At each location, 3 different speeds are tested: 0.5 μm/s (green), 1.0 μm/s (red), and 1.5 μm/s (blue). This result indicates that the mechanical response of the local matrix is largely rate-independent. **b**, Force-displacement relationship of five subsequent loading cycles at the same location in a 1.5 mg/mL collagen gel. This result indicates that the collagen matrix is predominately elastic in our study.

To check the uncertainty and local variability of our measurements, 10 independent measurements in 1.5 mg/mL collagen gel far from a cell are performed, as shown in Supplementary Figure 3a. Interestingly, while the force-displacement curves can differ significantly from location to location, the resultant relationship between the differential stiffness and the applied force are similar, especially in the nonlinear regime, as shown in Supplementary Figure 3b.

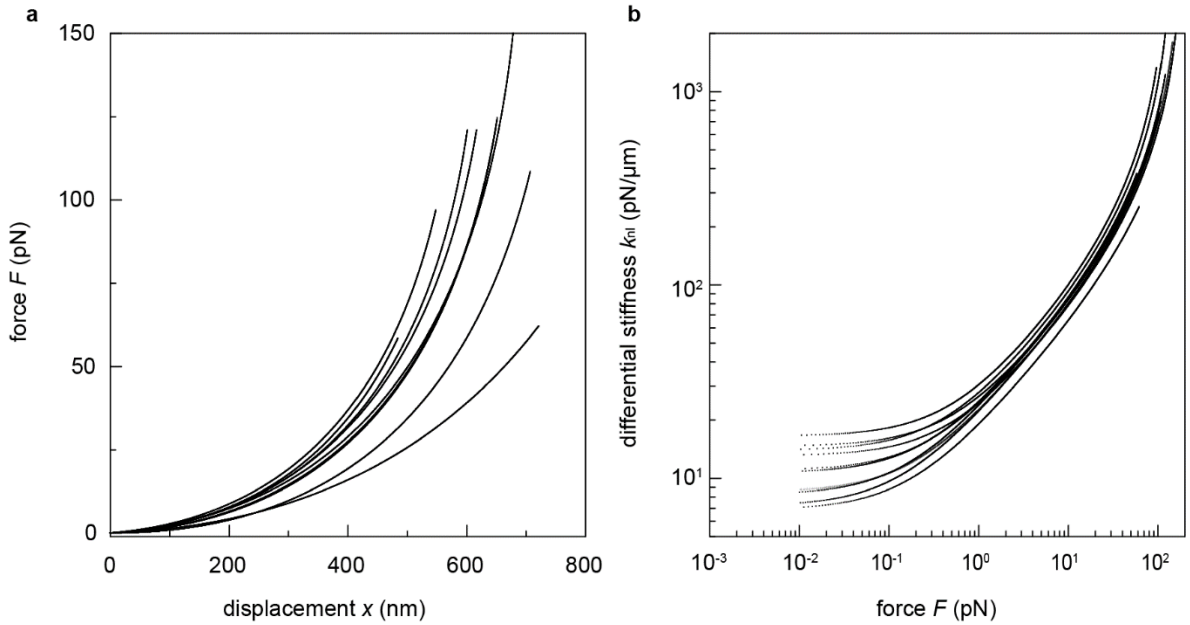

Supplementary Figure 3: Optical tweezers microrheology measurements in collagen samples. **a**, Ten independently measured force-displacement curves. **b**, Corresponding differential stiffness-force (k_{nl} vs. F) curves. The result indicates that although the collagen network is heterogeneous in linear stiffness, the nonlinear mechanics share a similar trend and collapse together.

Similar behavior is also observed in the cytochalasin D treated sample. We measure the nonlinear micromechanics at different distances to the cell in a 1.5 mg/mL collagen gel, with cell contractility inhibited by treatment of cytochalasin D, and plot the stiffness-force (k_{nl} vs. F) curves. We find that although the linear stiffness k_{lin} slightly increases closer to the cell, consistent with the observed increase in collagen density (Fig. 1f), the nonlinear mechanics at all distances approximately overlap for high forces, as shown in Supplementary Figure 4. This result indicates that, even if the matrix density varies slightly with distance, this density variation does not appear to affect the local nonlinear mechanical properties of the collagen gel. This observation may be explained by previous macrorheology experiments, where it was observed that the linear shear modulus depends on collagen density, while the differential shear modulus is largely determined by the stress level in the network with only a weak dependence on collagen concentration [1].

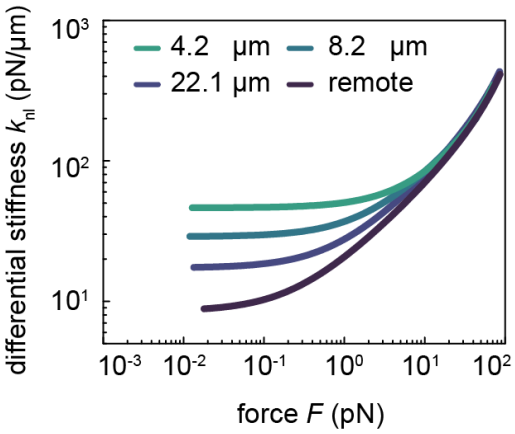

Supplementary Figure 4: Local nonlinear differential stiffness k_{nl} is plotted against the applied probe force F in a collagen matrix near a cytochalasin D treated cell. The difference in the linear stiffness k_{lin} is consistent with a change in fiber density, but all curves at different distances to the cell appear to asymptotically converge to the same response in the nonlinear regime.

1.3 Control experiments for the stiffness gradient measurements

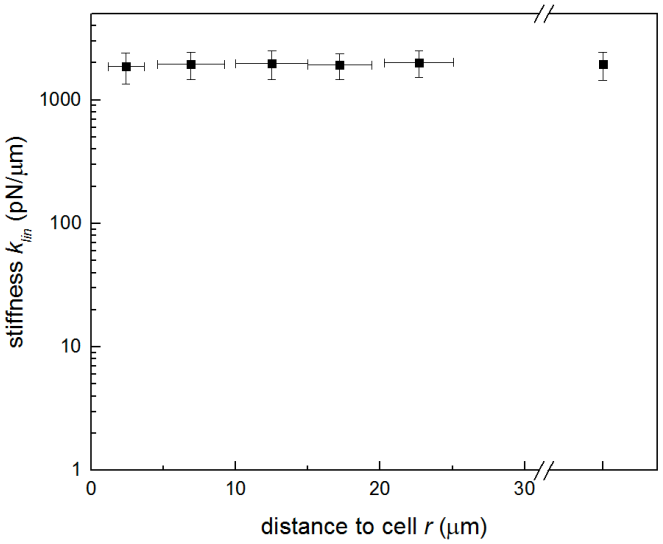

Supplementary Figure 5: Quantification of the linear stiffness k_{lin} of the local 3D matrix as a function of distance to the cell r in a linear RGD-alginate hydrogel.

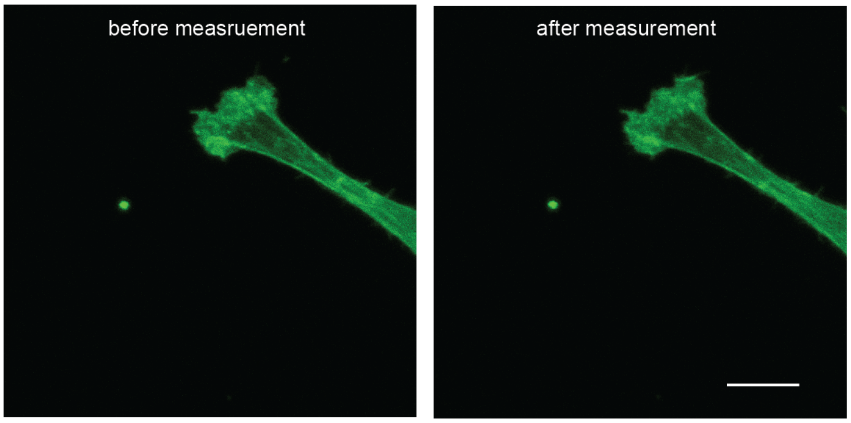

Supplementary Figure 6: F-actin cytoskeletal structures before and after active microrheology measurements. Scale bar: 10 μm.

1.4 Conversion from local force on the bead to local matrix stress

To use NSIM, we require a conversion between local force on the bead to local matrix stress (See Eq. 1 in the main text). This conversion is established by comparing nonlinear microrheology data with nonlinear macrorheology data. Specifically, we first shift the microrheology data (k_{nl} vs. F) in the vertical direction to align these data to the linear regime of the macrorheology data (K vs. σ), as shown in Supplementary Figure 6a. Subsequently, we shift the microrheology data in the horizontal direction to align these data with the nonlinear regime of the macrorheology data (Supplementary Figure 6a); the shift factor in the horizontal direction involves a multiplication factor, which defines the conversion from the local force on the bead to matrix stress. This gives a factor of ~2, ~3 and ~10 for collagen, fibrin, and Matrigel respectively. Note, to empirically find the conversion factor between force and stress by shifting, we use a comparable stiffening range of the microrheology and macrorheology data where they share a similar power-law behavior, as indicated by the solid symbols in the Supplementary Figure 6. Interestingly, we observe that k_{nl} becomes increasingly stiffer at large force as indicated by the pink symbols. However, this high stress regime is not accessible in macrorheology.

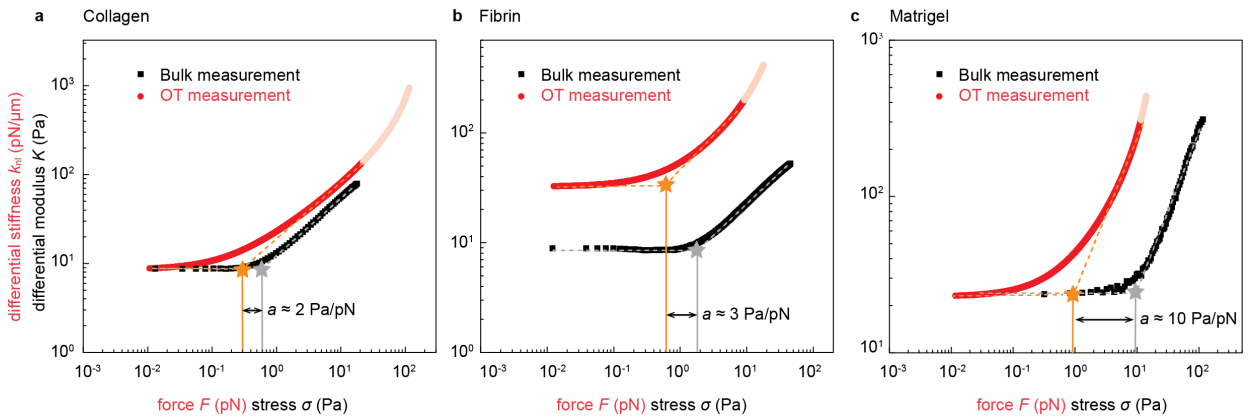

Supplementary Figure 7: Determination of conversion factors for NSIM between effective force and local matrix stress using active microrheology (Optical Tweezers) and bulk rheology, resulting in a factor of ~2, ~3 and ~10 for collagen, fibrin and Matrigel respectively.

1.5 Conversion from spring constant to Young's modulus

In a homogenous linearly elastic continuum, we can convert our measurement of local stiffness k_{lin} to a macroscopic modulus using the following relationship, $G = \frac{5-6\nu}{24\pi a(1-\nu)} k_{\text{lin}}$ [2], where G is the shear modulus, a is the radius of the bead, and ν is the Poisson's ratio; this reduces to the generalized Stokes relation under incompressibility assumption, $k_{\text{lin}} = 6\pi G a$, which is often used in the microrheology community [3-5]. If we use the Generalized Stokes relation to convert k_{lin} to a macroscopic shear modulus far from the cell in Fig. 1f, we would estimate G to be roughly 0.2 Pa. However, there are several important reasons why we decided not to report our data in terms of such a macroscopic material property. At the scale of the bead, the network is intrinsically highly heterogeneous and the local mechanical properties may be significantly different from a macroscopic measurement. This heterogeneity precludes a linear homogenous continuum description of the matrix near the cell, and therefore the generalized Stokes relation may not be valid. In addition, in the vicinity of the cell, contractile stresses stiffen the medium in a way that depends strongly on the distance to the cell, which further exacerbates a simple conversion between local stiffness and the macroscopic material properties. Note that these are not limitations of our specific microrheology technique, but they are intrinsic to any local characterization of the micromechanics of the ECM at the scale of a cell.

Importantly, since we aim to understand micromechanical cell-matrix interactions, we prefer to provide a model-independent measure that is relevant at the scale of the cell. Nonetheless, an intrinsic local modulus can be obtained by dividing k_{lin} by the radius of the bead. However, such a local modulus only relates to a material's property like the Young's modulus for a perfectly homogenous linear elastic continuum. Therefore, we report the data as we measure it directly from microrheology.

Supplementary Table 1: The effective force F_{eff} determined with NSIM using the data in Fig 4a

Collagen		Fibrin		Matrigel	
r (μm)	F_{eff} (pN)	r (μm)	F_{eff} (pN)	r (μm)	F_{eff} (pN)
2.6	114.50	3.3	10.50	3.4	14.28
5.5	19.68	8.0	2.00	6.9	7.60
10.5	5.40	15.5	0.26	14.8	1.47
17.2	1.43	24.4	0.03	24.5	0.59
28.9	0.44			33.1	0.43

1.5 General Manual of NISM

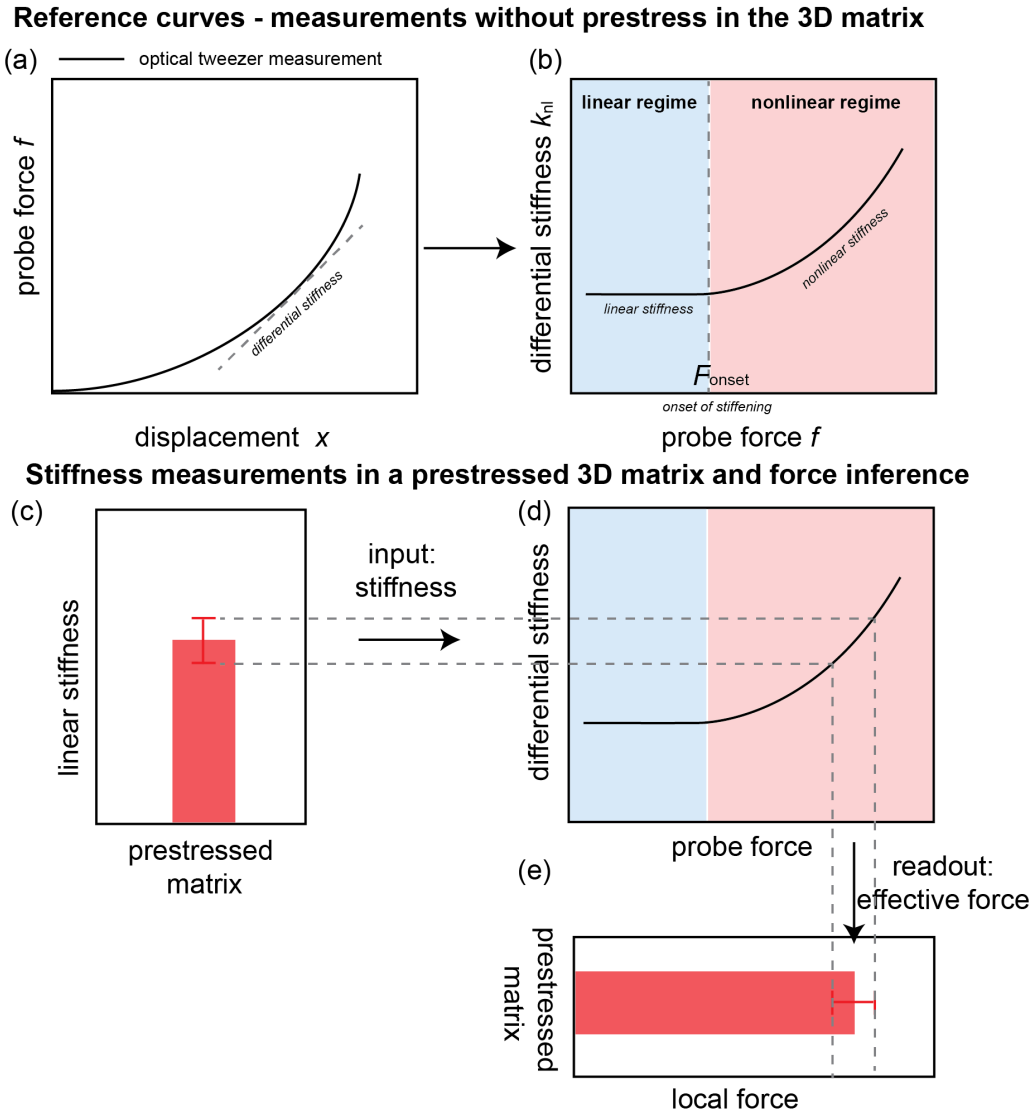

Supplementary Figure 8: General procedure of NSIM

1. To measure the local prestress inside the matrix, we first need to generate a reference curve for the specific matrix. To do so, we pre-mix particles with a size larger than the matrix mesh size in the three-dimensional matrix without cell induced stress. In 1.5 mg/mL collagen matrix we use particles with a diameter of 4.5 μm. Subsequently, the reference force-displacement relationship of the matrix is measured using optical tweezers by dragging the particle unidirectionally with a constant speed (1 μm/s) for 1 μm in distance, at a random direction.
2. Since biopolymer matrix is typically heterogeneous, especially at the microscale, it is necessary to perform average over multiple measurements (n>10) to obtain a reliable force-displacement relationship at the reference state, as shown in Supplementary Fig. 8a.

3. The differential stiffness of the matrix is defined as the slope in the force-displacement relationship, as indicated by the gray dashed line in the Supplementary Fig. 8a. Then we calculate the differential stiffness of the matrix, as:

$$k_{nl} = \frac{df}{dx},$$

where f is the applied force and x is the particle displacement. k_{nl} is plotted against f, as shown in Supplementary Fig. 8b. This relationship is used later as a reference curve to readout the local forces induced by a contracting cell.
4. To measure the matrix stiffness near a contracting cell, we embed the same type of particles together with living cells in the matrix. A low cell density (10^4 /mL) is used to avoid the interaction between cells and between cell-generated stress fields. The particle density is optimized to maximize the spatial resolution without affecting cell viability.
5. After the cells spread out in the matrix, we drag a particle away from the cell with the same speed and total distance, similar to **step 1**, and obtain a local force-displacement relationship of the matrix near the cell. This relationship can also be obtained after cytochalasin D treatment with the same approach.
6. Similar to **step 3**, we use this local force-displacement relationship to calculate the differential stiffness of the local matrix and plot it against the applied force. Then we take the local linear stiffness k_{lin} of the matrix, defined as the small force limit of $k_{nl}(F)$.
7. Repeat **steps 5-6** for all the particles near the cell to obtain a map of linear matrix stiffness.
8. To infer the local stress from the local stiffness, we read the force value from the reference curve obtained in **step 3** (Supplementary Figs. 8c-e), by finding the force value corresponding to the same stiffness value on the reference curve.
9. To convert the local force to the local stress in the matrix, we need to determine the proportionality factor a in Equation 1 in the main text. We determine the proportionality factor a by assuming that nonlinearity sets in at a similar stress σ^* at the macroscopic and the microscopic level. In practice, we adjust a to match the low- and high-stress asymptotes, in a log-log plot, of the macroscopic differential shear modulus $K(\sigma_{macro})$ to those of the microrheology curve $k_{nl}(F)$ (Figs. 2c-e, Supplementary Figs. 7 and 13). With the pre-factor and inferred force in **step 8**, the local stressed is calculated according to Equation 1 in the main text.
10. Repeat **steps 8-9** so that the local stiffness map in **step 7** is converted to a local stress map.

2 Simulation methods and parameter choices

The simulation results presented in Figure 3 of the main text are obtained with a lattice model of nonlinear springs. In this model, nonlinear springs of unit rest length are arranged on the edges of a 3D face-centred cubic lattice, and the positions of the vertices thus represent the degrees of freedom of the system. To capture the stiffening behavior of the network, we choose a nonlinear force-extension relation for these springs as:

$$f(x) = \exp(\mu\, x) - 1 \tag{1}$$

which results in an exponential stress-strain relationship at macroscopic scales, consistent with experimental observations in collagen [1]. At large forces, f, this choice yields a power-law dependence of local differential stiffness on tension: $k_{\mathrm{nl}} = df/dx \propto f$. Other types of nonlinearities are considered in Sec 3.2.

We simulate a large spherical region of the network of radius R with fixed boundary conditions. The contractile cell is modelled by a rigid ellipsoid replacing a portion of the network in the center. All lattice nodes that are initially inside the ellipsoid are constrained to translate and rotate as a single rigid body, which can be affinely deformed to simulate contractile forces. Force and torque balance over the rigid body are ensured by including its bulk rotational and translational degrees of freedom to the energy minimization.

To capture network disorder, a fraction of the springs is randomly suppressed. This construction will result in substantial mechanical heterogeneities as well as non-affine network deformations, which are characteristic of fibrous networks [6]. However, a finite-size artefact occurs when a straight chain of springs remains that connects the cell at the center of the spherical network to the system's boundary. At large deformation, such straight lines tend to concentrate all the stress as they stiffen dramatically. Since 3D numerical simulations are limited in size, we choose to limit the length of such alignments to a given "fiber length" $L_f < R$. Specifically, for each line of aligned edges in the initial configuration, we randomly choose a starting point, and remove one spring every $L_f + 1$ edges, thereby ensuring that no straight line connecting the cell to the system's boundary remains.

Local stiffnesses are obtained by measuring the response to point forces, exerted on selected lattice nodes, and directed towards the center of the ellipse. The "remote" force-displacement curve in Figure 3b of the main text, which serves as a reference for NSIM, is obtained in a similar system with no contractile cell, and with the probe placed at the center of the network.

Local stress at a lattice node is defined as minus the dipole moment of the forces exerted by nearby nodes, divided by the unit cell volume. This construction is consistent with a macroscopic definition of stress.

Macrorheological calibration, as discussed in Figure 2 of the main text, is performed on a large system with periodic boundary conditions, in the absence of cells or probes. The network is stressed by affinely deforming the periodic boundary conditions vectors, in a Lees-Edwards fashion. The stress is evaluated using the discrete mean-stress theorem [7].

This system is simulated in C++14. Mechanical equilibrium is obtained by minimizing the total energy using the GNU Scientific Library [8] BFGS2 implementation of the Broyden-Fletcher-Goldfarb-Shanno algorithm. Data analysis and visualization are performed in Python2 using the SciPy [9], Matplotlib [10] and Mayavi2 [11] packages.

In Figure 3 of the main text, we use the following parameters: system radius $R = 50.5$, spring stiffness parameter $\mu = 50$, and fiber length $L_f = 10$. The cell has ellipse aspect ratio $5:1:1$, with its long axis with length 14.2 along the (111) lattice direction. The cell is contracted by 50% along its long axis. We probe the linear stiffness at each of the 614 points that are present in the plane perpendicular to the $(1/\sqrt{7}, \sqrt{6/7}, 0)$ vector (which includes the cell's long axis) and located at a distance > 5 from the system's boundary to avoid edge effects. These points are displayed in Figure 3a of the main text. Local linear stiffness is measured by exerting a force strong enough to displace the probe node by 10^{-3}, small enough to be consistently in the linear response regime, yet large enough to prevent numerical imprecision. The "remote" reference curve is obtained by measuring the displacement in response to forces ranging from 10^{-2} to 10^{5}, in 22 logarithmic increments, and we used spline-fitting on the force-displacement curve in log-log space. This allows us to robustly evaluate the nonlinear differential stiffness $k_{\mathrm{nl}}(F)$, which we average over 20 realizations of the network. The macrorheological calibration system size is 40^3, with isotropic strain γ varying logarithmically from 10^{-5} to 0.46, and similar log-log spline-fitting is applied to macrorheological stress-strain curve. The consequences of this choice of geometry are discussed in Sec 3.5.

3 Robustness of NSIM

In this Section we provide further support for the robustness of our stress inference method in numerical simulations, by considering additional geometries, which are different from the case of stresses induced by an elliptic cell presented in Figure 3 of the main text.

3.1 Homogeneously prestressed systems

We first consider the case of a system where the stress is spatially homogeneous, and originates from the deformation of the boundary of the system. We consider a spherical system with fixed boundary conditions, with a deformation according to a strain:

$$\begin{pmatrix} \gamma & 0 & 0 \\ 0 & -\gamma/2 & 0 \\ 0 & 0 & -\gamma/2 \end{pmatrix} \tag{2}$$

where the x-direction is also the force direction, which we take to be the (111) lattice direction. This geometry of rotationally symmetric shear strain corresponds to the strain in a linear elastic material with a spherically contractile cell.

We present the results for these simulations in Supplementary Figure **9**, showing excellent agreement between the inferred stress and its measured value, up to a proportionality factor of roughly ~ 0.3. This shows that NSIM accurately captures stress variations in a disordered networks, and that our calibration allows us to capture stresses within a factor of 2-3 depending on the geometry of the strain field. This accuracy is similar to other experimental errors such as the typical experiment-to-experiment variation of macrorheological protocols on biopolymer networks.

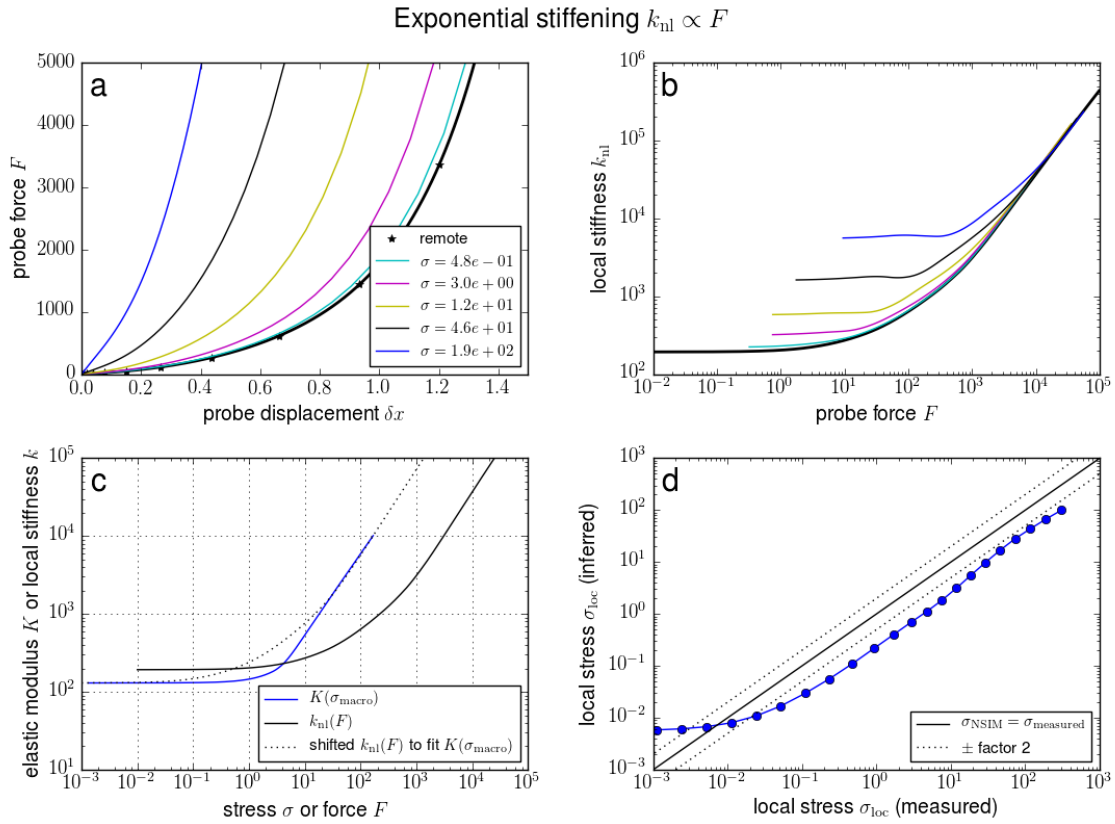

Supplementary Figure 9: Results for NSIM in a homogeneously prestrained network. **a**, Nonlinear force-displacement curves for varying pre-stress. **b**, Nonlinear stiffening curves (same colors as in **a**). **c**, Calibration using macrorheology data: the prefactor for NSIM is obtained by aligning the micro- and macrorheological curves, as illustrated in Figure 2 of the main text. **d**, Inferred local stress versus direct measurement, showing proportionality at large stress. Parameters for these simulations: $\mu = 100$, $L_f = 12$, $R = 15.5$.

3.2 Other types of nonlinearities

In most simulations in this article, we employ a specific type of nonlinearity for our fibers, with an exponential force-extension relation as described in Eq. (1), for which $k_{\mathrm{nl}}(F) \sim F$ at large forces. However, as shown in Sec. 4 in a simplified geometry, NSIM applies more generally to any nonlinear system with a power-law dependence between k_{nl} and F. In parallel with our study of homogeneously prestressed systems in Sec. 3.1, we demonstrate here that NSIM works for two other types of nonlinearities:

- Square-root stiffening (Fig. **10**):

$$f(x) = \begin{cases} \mu x, & x \leq 0 \\ \mu x\left(1 + \frac{\mu x}{4}\right), & x > 0 \end{cases} \tag{3}$$

  In this mildly nonlinear case, the local stiffness scales as $k_{\mathrm{nl}} \propto \sqrt{F}$ at large tension, with a crossover occurring around $F = 1$.

- Worm-like-chain nonlinearity (Fig **11**):

$$f(x) = \mu x \frac{1 - \mu x/4}{(1 - \mu x/2)^2} \tag{4}$$

  In this strongly nonlinear case, the local stiffness scales as $k_{\mathrm{nl}} \propto F^{3/2}$ at large tension, with a crossover occurring around $F = 1$. Note the divergence of the force-extension relation at a finite extension $x_\infty = 2/\mu$. This force-extension relationship is inspired by the Worm-Like-Chain model for entropic elasticity of semiflexible polymers [6], with the same asymptotic stiffening behavior as a Worm-Like-Chain, but with a simplified crossover between the linear and nonlinear regimes.

We performed simulation with these two choices of force-extension curves. In both cases, the stress inferred by NSIM asymptotically approaches the measured local stress up to a prefactor of order one (Figs. **10d** and **11d**), thereby demonstrating the applicability of NSIM to broad variety of systems.

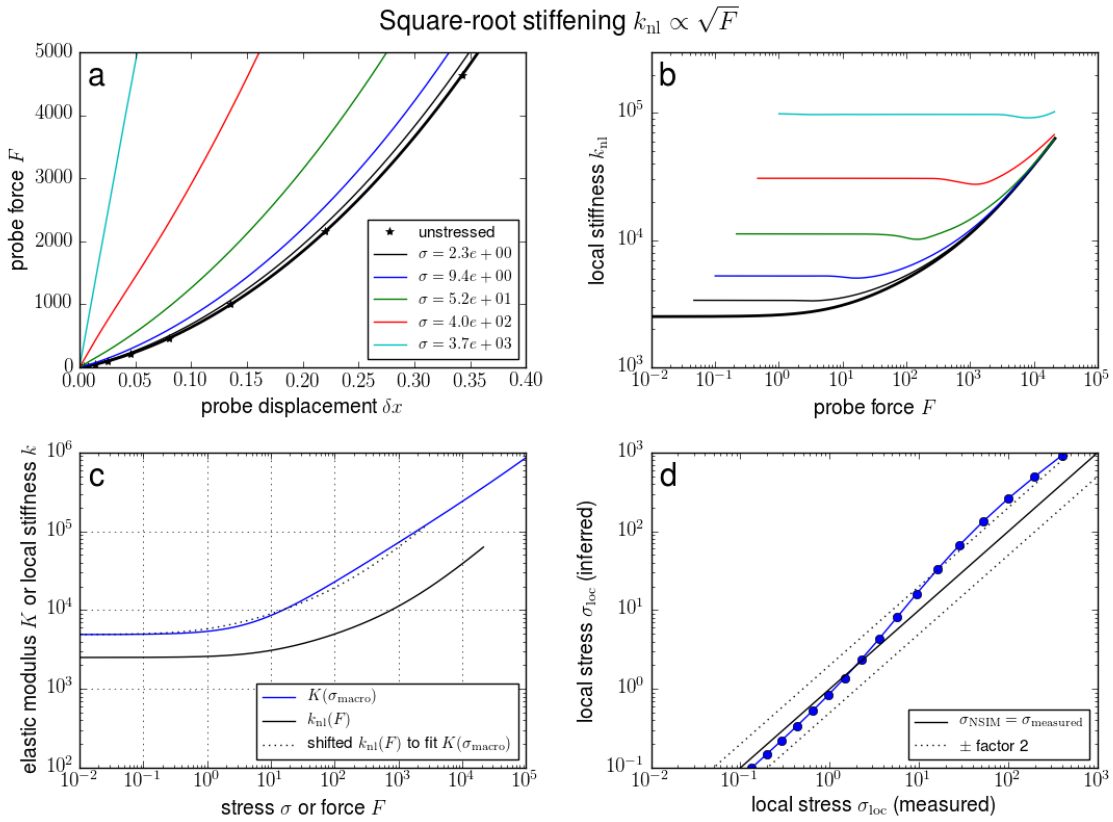

Supplementary Figure 10: Results for NSIM in a homogeneously prestrained network with square-root nonlinearity, as described in Eq. (3) (same panels as Fig **9**). Parameters: $\mu = 1000$, $L_f = \infty$ (regular network), $R = 15.5$.

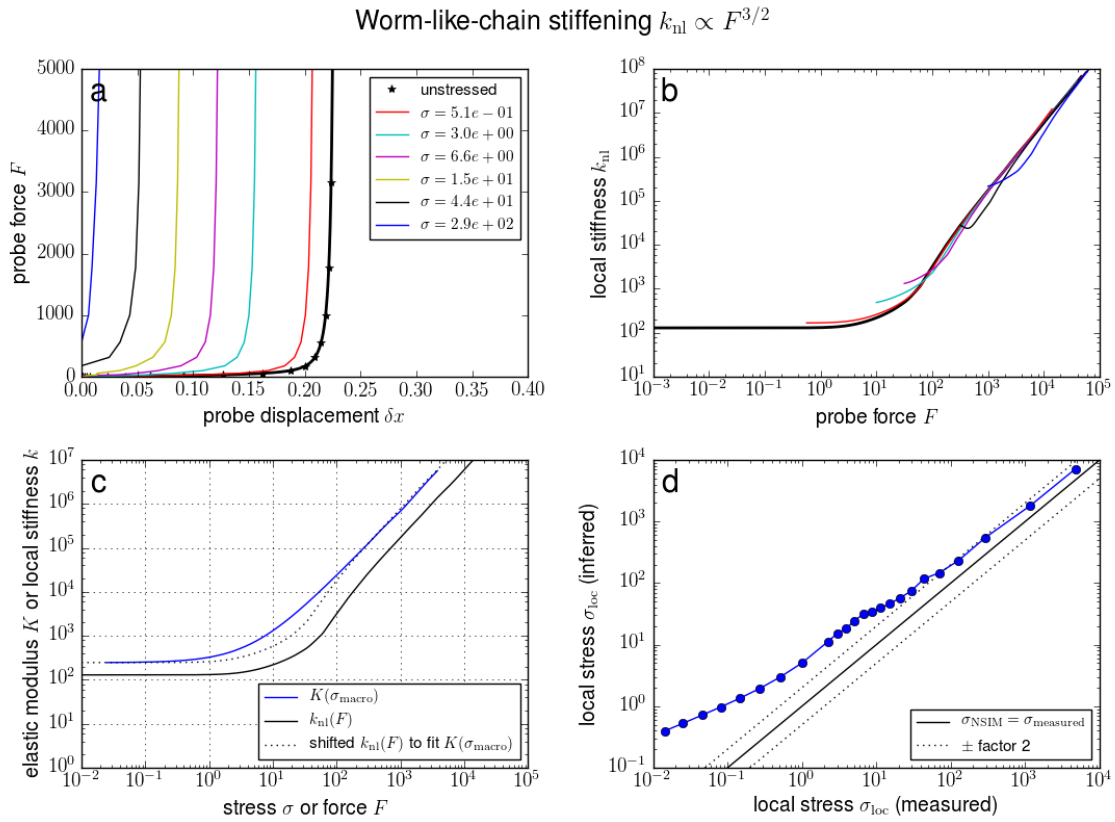

Supplementary Figure 11: Results for NSIM in a homogeneously prestrained network with square-root nonlinearity, as described in Eq. (3) (same panels as Fig **9**). Parameters: $\mu = 50$, $L_f = \infty$ (regular network), $R = 4.5$ (the finite-extension force divergence causes convergence issues at large force that limit the size of the system).

3.3 Isotropically contractile cell

Next, we consider the case of a spherically symmetric contractile cell, modeled as a rigid sphere that shrinks isotropically (Supplementary Figure **12**a). We perform NSIM on a 1000 random points in the network, whose distances to the cell center are uniformly distributed in log scale. These results are presented in Supplementary Figure **12**c, showing excellent agreement between inferred and measured stress. The stress is long-ranged and decays as r^{-2} with distance to the cell (Supplementary Figure **12**e), consistent with previous results and simulations of elliptic cells presented in the main text.

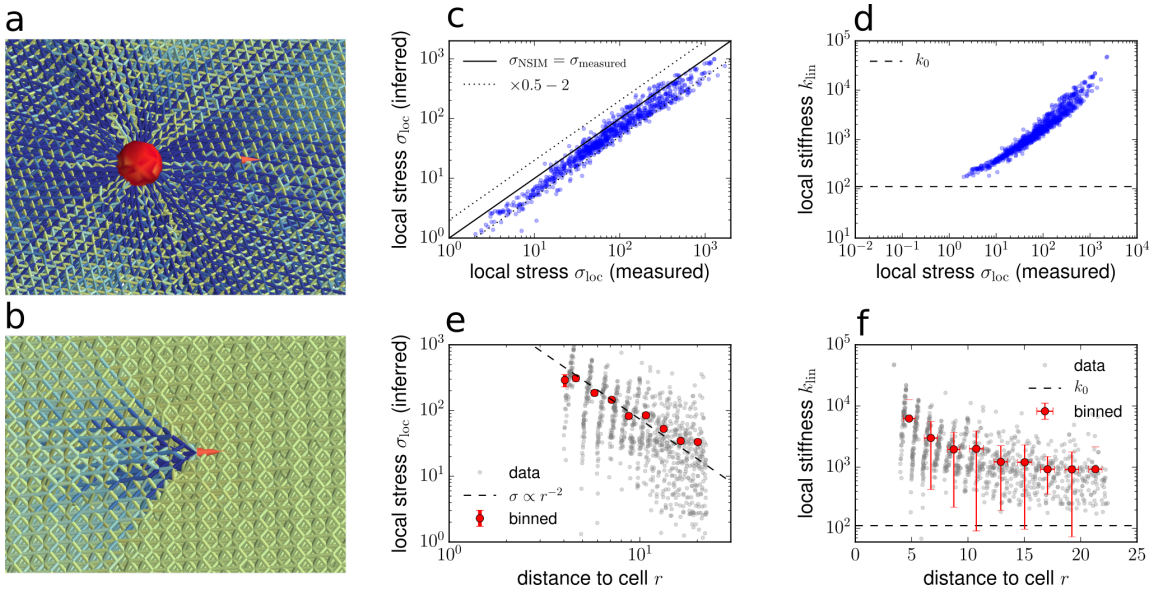

Supplementary Figure 12: NSIM in a spherically symmetric stress field. **a,** Here the cell model consists of a rigid sphere of radius $R_{\rm cell} = 5.1$ that shrinks by 55% in a spherical system of radius $R = 25.5$, with fixed boundary conditions. Network parameters: $L_{\rm f} = 22$, $\mu = 50$. **b,** The "remote" reference curve is obtained in an unstressed network. **c,** Stress inferred with NSIM *vs* measured stress, for a 1000 random points in the network. The agreement between the two measures is good over three decades of stress. **d,** Linear stiffness *vs* stress. **e,** Stress decay away from the cell. While the signal-to-noise ratio is high due to the mechanical disorder intrinsic to our modelled networks, binning and averaging yield results consistent with rope-like force transmission. **f,** Decay of the local stiffness away from the cell.

3.4 NSIM captures local stress fluctuations

In this section we show that NSIM captures not only the average stress, but also local stress fluctuations due to heterogeneity in the local mechanical properties. To demonstrate this, we consider our simulations in the case of an isotropically contractile cell (Sec 3.3) and analyze the correlations between three data sets: distances to cell r, local linear stiffness $k_{\rm lin}$, and local stress $\sigma_{\rm loc}$ (obtained by direct measurement). We find the following Pearson linear correlation coefficients ρ (for log-log correlations):

$$\rho(k_{\rm lin}, r) = -0.63$$
$$\rho(\sigma_{\rm loc}, r) = 0.56$$
$$\rho(k_{\rm lin}, \sigma_{\rm loc}) = 0.97$$

In other words, both k_{lin} and σ_{loc} fluctuate strongly and are not determined by the distance to the cell, but stress fluctuations are strongly correlated with local stiffness fluctuations.

Performing a log-log linear regression of the measured local stress σ_{loc} with that obtained using NSIM, we find that the best power-law fit has exponent 1.04 and prefactor 0.567 (the prefactor here is with isotropic prestrain for the calibration; see discussion in Sec 3.5). This is consistent with the ideal case for NSIM where the exponent would be 1, showing that NSIM also captures stress fluctuations due to mechanical heterogeneity.

3.5 Macrorheological geometry and NSIM prefactor

Calibration is done with a macrorheology simulation, measuring the stress response to a bulk strain with a system size of 40^3 with periodic boundary conditions. Tensorial stresses are measured using the mean stress theorem.

If $\hat{\gamma} = \gamma \hat{e_\gamma}$ is the strain matrix, we define the scalar stress as $\sigma = \text{Tr}(\hat{\gamma} \cdot \hat{\sigma})/||\hat{\gamma}||$ and the differential modulus as:

$$K = \frac{\partial \sigma}{\partial \gamma}$$

using a logarithmic spline interpolation to differentiate.

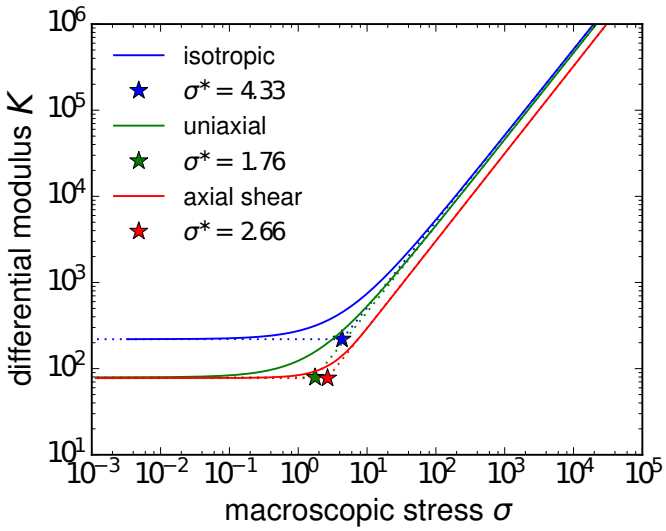

Supplementary Figure 13: Macrorheology curves for calibration. Different strain geometries lead to different values of σ^*, which impacts the final value of the force-stress conversion factor. Empirically, we find that an isotropic dilation (blue curve) gives the most accurate result for the conversion factor. The green curve shows the case of a uniaxial dilation, and the red curve corresponds to uniaxial dilation with compensating compression in the other two directions to ensure volume conservation at linear level. A spherical contractile cell in linear elasticity corresponds to the latter case.

4 Proof of NSIM within a minimal 1D model

In the main text we mentioned that the NSIM correspondence between local force and local stress at equivalent stiffness becomes exact in the case of power-law stiffening of the network. To establish this result, we employ a minimal model, consisting of two nonlinear springs describing the network response.

4.1 Model

Our minimal model (Supplementary Figure **14**) consists of two nonlinear springs in series, with unit rest length and a generic force-extension relation $\frac{1}{2}f(\delta)$ (the $1/2$ being for convenience of notation). The network prestress is modeled by a displacement of the two boundary points by γ (fixed strain), resulting in a stress

$$\sigma(\gamma) = f(\gamma) \tag{5}$$

at the central point. The force exerted by optical tweezers results in a displacement of the central point of a distance x, corresponding to a force

$$F(x,\gamma) = \frac{f(\gamma+x) - f(\gamma-x)}{2} \tag{6}$$

In particular, in the absence of prestress, we define the reference force-displacement curve for the probe,

$$F_{\text{ref}}(x) = F(x,\gamma=0) = \frac{f(x) - f(-x)}{2} = \tilde{f}(x) \tag{7}$$

where $\tilde{f}$ is the odd part of f.

As discussed in the main text, the experimentally measurable quantities are $F(x,\gamma)$ for an unknown prestress. We define as before the linear stiffness in the pre-strained state:

$$k_{\text{lin}}(\gamma) = \frac{\partial F}{\partial x}(x=0,\gamma) = f'(\gamma) \tag{8}$$

and the nonlinear differential stiffness in the absence of pre-stress:

$$k_{\text{nl}}(x) = \frac{\partial F}{\partial x}(x,\gamma=0) = \frac{f'(x) + f'(-x)}{2} = \tilde{f}'(x) \tag{9}$$

4.2 Mathematical formulation of NSIM correspondence

The idea of Nonlinear Stress Inference Microscopy is that the network's stiffness depends on its stress state (*i.e.*, f is nonlinear) such that we can establish a correspondence between the force-induced stiffening curve k_{nl} and the stress-induced stiffening curve k_{lin}.

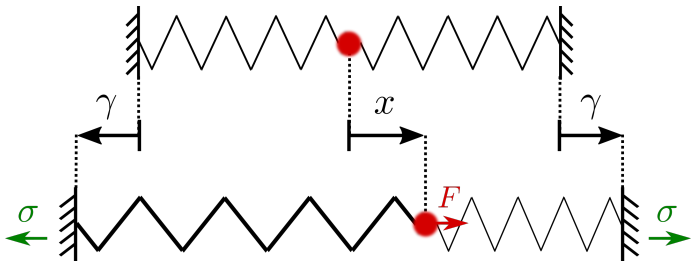

Supplementary Figure 14: A minimal model for our microrheological system. Two nonlinear springs describe the network surrounding a bead. Starting from an unstressed reference configuration (top), the cell-generated prestress, σ, induces a symmetric elongation of the two springs by γ, and the force F exerted by the optical tweezer results in a displacement x of the bead.

Specifically, to each pre-strain γ we associate an *effective displacement* $x_{\text{eff}}(\gamma)$ corresponding to the same differential stiffness, such that

$$k_{\text{lin}}(\gamma) = k_{\text{nl}}\left(x_{\text{eff}}(\gamma)\right) \tag{10}$$

hence

$$x_{\text{eff}}(\gamma) = k_{\text{nl}}^{-1}\left(k_{\text{lin}}(\gamma)\right) \tag{11}$$

We are interested, however, in mechanical quantities F and σ rather than in the associate geometrical quantities x and γ. We thus define the effective local force $F_{\text{eff}}(\sigma)$ that corresponds to the same differential stiffness as the local stress σ:

$$F_{\text{eff}}(\sigma) = F_{\text{ref}}\left(k_{\text{nl}}^{-1}\left(k_{\text{lin}}\left(\gamma(\sigma)\right)\right)\right) \tag{12}$$

Our stress microscopy technique requires that $F_{\text{eff}}(\sigma) \propto \sigma$; we now study the conditions under which this identity holds.

Mathematically, in terms of the generic nonlinear force-extension relation of the springs, we have:

- $$\sigma(\gamma) = f(\gamma) \tag{13}$$
- $$k_{\text{lin}}(\gamma) = f'(\gamma) \tag{14}$$
- $$F_{\text{ref}}(x) = \frac{f(x) - f(-x)}{2} = \tilde{f}(x) \tag{15}$$

  where $\tilde{f}$ is the odd part of f.

•

$$k_{\mathrm{nl}}(x) = \tilde{f}'(x) \tag{16}$$

therefore:

$$F_{\mathrm{eff}}(\sigma) = \left[\tilde{f} \circ \left(\tilde{f}'\right)^{-1} \circ f' \circ f^{-1}\right](\sigma) \tag{17}$$

Schematically:

$$\sigma \overset{f^{-1}}{\longmapsto} \gamma \overset{f'}{\mapsto} k_{\mathrm{lin}} \sim k_{\mathrm{nl}} \overset{\left(\tilde{f}'\right)^{-1}}{\longmapsto} x_{\mathrm{eff}} \overset{\tilde{f}}{\mapsto} F_{\mathrm{eff}} \tag{18}$$

4.3 Conditions for NSIM

The question we need to address is: how does the composite function $F_{\mathrm{eff}} = \tilde{f} \circ \left(\tilde{f}'\right)^{-1} \circ f' \circ f^{-1}$ compare to the identity function? When this is the case, we will be ensured to have: $F_{\mathrm{eff}}(\sigma) \propto \sigma$. which is the requirement for NSIM.

Note first that in order to be able to infer an effective force F_{eff}, the values taken by k_{nl} and k_{lin} should be the same. In particular, this implies that f should have a *nonlinear odd* component, such as a cubic or quintic term. Otherwise, there is no stiffening under displacement of the probe (as the weakening of one side exactly compensates the stiffening of the other), and thus no inference is possible as $\tilde{f}$ is not invertible. In contrast, if f is odd, $F_{\mathrm{eff}}(\sigma) = \sigma$ for all values of σ; however this case corresponds to a material for which the nonlinear response under compression and tension is the same, which does not correspond to any physical situation. Also $\tilde{f}'$ is even by construction, and thus invertible only on $\mathbb{R}_+$, *i.e.*, probe forces F and $-F$ are indistinguishable.

4.3.1 Weakly nonlinear regime

Next we consider a generic case where all terms of the Taylor expansion of f are nonzero:

$$f(\delta) = \delta + \frac{a_2}{2}\delta^2 + \frac{a_3}{3}\delta^3 + \dots \tag{19}$$

where the first coefficient is set to unity (which gives the stiffness scale, *i.e.* $k_0 = 1$). In this case, we have, to first nonlinear order:

$$f'(\delta) = 1 + a_2\delta + \dots \tag{20}$$

$$\tilde{f}(\delta) = \delta + \frac{a_3}{3}\delta^3 + \dots \tag{21}$$

$$\tilde{f}'(\delta) = 1 + a_3\delta^2 + \dots \tag{22}$$

thus

$$f^{-1}(t) = t - \frac{a_2}{2}t^2 \tag{23}$$

$$\left(\tilde{f}'\right)^{-1}(k) = \sqrt{\frac{k-1}{a_3}} + \dots \tag{24}$$

and so

$$F_{\text{eff}}(\sigma) = \left[\tilde{f} \circ \left(\tilde{f}'\right)^{-1} \circ f' \circ f^{-1}\right](\sigma) = \sqrt{\sigma} + \left(\frac{a_3}{3} - \frac{a_2}{4}\right)\sigma^{3/2} + \dots \tag{25}$$

Hence in the weakly nonlinear regime $F_{\text{eff}}(\sigma) \sim \sqrt{\sigma}$, precluding an accurate inference of stress by this method. This is due to the difference in symmetry between force and stress, as discussed in Figure 2 of the main text.

4.3.2 Strongly nonlinear regime

We now examine the conditions for proportionality between stress and effective force in the strongly nonlinear regime. We make the following assumptions regarding the stiffening function f characteristic of the material:

- Diverging stiffness:

$$\lim_{x \to x_\infty} f'(x) = \infty \tag{26}$$

  where x_∞ stands for either a finite maximum elongation (Worm-Like-Chain-like divergence) or infinity. This assumption excludes linear and strain-softening materials for instance.

- Compression-extension ratio:

$$\lim_{x \to x_\infty} f(x)/f(-x) = -c \tag{27}$$

  where $0 \leq c < \infty$. The number c is a characteristic of the material: $c = 0$ for a material which buckles and yields under compression, and $c = 1$ for an odd force-extension relation. We also define $q = (1+c)/2$, such that:

$$\tilde{f}(x) \underset{x \to x_\infty}{\sim} q f(x) \tag{28}$$

  with $q = 1/2$ for a buckling material.

Under these assumptions, we now derive a functional relation that the force extension curve f needs to obey to exactly satisfy NSIM conditions in the strongly nonlinear regime. First we define $S(k) = f\left(f'^{-1}(k)\right)$ and $\tilde{S}(k) = \tilde{f}\left(\tilde{f}'^{-1}(k)\right)$, such that:

$$\sigma = S(k_{\text{lin}}) \tag{29}$$

and

$$F = \tilde{S}(k_{\text{nl}}) \tag{30}$$

Hence we can rewrite Eq. 25 as

$$F_{\text{eff}}(\sigma) = \tilde{S}\left(S^{-1}(\sigma)\right) \tag{31}$$

The requirement for our NSIM correspondence is that $F_{\text{eff}}(\sigma) \propto \sigma$, which translates to $\tilde{S}\left(S^{-1}(\sigma)\right) = b\sigma$ for some stress-force proportionality constant b. For this proportionality to hold in the strongly

nonlinear asymptotic regime $k \to \infty$ limit (under the assumption that the network stiffens under tension, *i.e.* Eq. (26)), we need to have

$$\frac{S(k)}{\tilde{S}(k)} \xrightarrow[k\to\infty]{} b \qquad ; \qquad 0 < b < \infty \tag{32}$$

Equation (28) implies that

$$\tilde{f}'^{-1}(k) \underset{k\to\infty}{\sim} f'^{-1}(k/q) \tag{33}$$

Combining this with Eq. 32, we get

$$\tilde{S}(k) \underset{k\to\infty}{\sim} qS(k/q) \tag{34}$$

The condition that S and $\tilde{S}$ be proportional (Eq. (32)) thus implies:

$$\boxed{S(k) \underset{k\to\infty}{\sim} bqS(k/q)} \tag{35}$$

Of course, if $q = 1$ (asymptotically odd function), this equation only implies $b = 1$, which we already knew (as discussed at the start of Sec 4.3). For any other value of q, including the case of a buckling material, Eq. (35) is highly constraining: Assuming a physically reasonable behavior for the material[1], this functional relationship indeed implies a power-law behavior prescribed by the value of the proportionality constant b:

$$S \underset{k\to\infty}{\sim} Ak^{\alpha} \tag{36}$$

with

$$\alpha = 1 + \frac{\log b}{\log q} \tag{37}$$

Note that the values of q and α, both of which are physically measurable and meaningful, set the value of the constant b.

4.3.3 Consequences on f

Recalling the definition of $S(k) = f\left(f'^{-1}(k)\right)$ (Eq. (29)), the power law form (rewriting Eq. (36) in terms of f^{-1}) implies that :

$$f'^{-1}(k) \underset{k\to\infty}{\sim} f^{-1}(Ak^{\alpha}) \tag{38}$$

We invert this equation to arrive at

$$f'(x) \underset{x\to x_\infty}{\sim} \left[\frac{1}{A} f(x)\right]^{\frac{1}{\alpha}} \tag{39}$$

[1]More precisely Eq. (35) implies that $S(k) = k^{\alpha}\phi(\log k)$, where ϕ is a generic $\log(q)$-periodic function. It is thus natural to assume that ϕ is a constant, the alternative being that the stiffness curve shows some kind of non-trivial self-similar structure.

This differential equation on f has the following solution, depending on the value of α:

$$f(x) \sim \begin{cases} x^{\frac{\alpha}{1-\alpha}} & 0 < \alpha < 1 \\ \exp(\mu x) & \alpha = 1 \\ (x_\infty - x)^{-\frac{\alpha}{\alpha-1}} & \alpha > 1 \end{cases} \tag{40}$$

These solutions include standard models for force-extension relations of individual biopolymers, such as the Worm-Like-Chain model ($\alpha = 2$) or exponential stiffening ($\alpha = 1$ as in the numerical simulations presented in the main text).

In summary, we have shown that the effective force F_{eff} becomes exactly proportional to the local stress σ_{loc} in the strongly nonlinear regime if, and only if, the stiffness-tension relationship of the springs asymptotically behaves as a power-law.

References

1. Licup AJ, Münster S, Sharma A, Sheinman M, Jawerth LM, Fabry B, Weitz DA, & MacKintosh FC (2015) Stress controls the mechanics of collagen networks. *PNAS* 112(31):9573-9578.
2. Selvadurai A (2016) Indentation of a spherical cavity in an elastic body by a rigid spherical inclusion: influence of non-classical interface conditions. *Continuum Mech. Thermodyn.* 28(1-2):617-632.
3. Hu J, Jafari S, Han Y, Grodzinsky AJ, Cai S, & Guo M (2017) Size- and speed-dependent mechanical behavior in living mammalian cytoplasm. *PNAS* 114(36):9529-9534.
4. Mizuno D, Tardin C, Schmidt CF, & MacKintosh FC (2007) Nonequilibrium mechanics of active cytoskeletal networks. *Science* 315(5810):370-373.
5. Guo M, Ehrlicher Allen J, Jensen Mikkel H, Renz M, Moore Jeffrey R, Goldman Robert D, Lippincott-Schwartz J, Mackintosh Frederick C, & Weitz David A (2014) Probing the Stochastic, Motor-Driven Properties of the Cytoplasm Using Force Spectrum Microscopy. *Cell* 158(4):822-832.
6. Broedersz CP & MacKintosh FC (2014) Modeling semiflexible polymer networks. *Rev. Mod. Phys.* 86(3):995.
7. Ronceray P & Lenz M (2015) Connecting local active forces to macroscopic stress in elastic media. *Soft matter* 11(8):1597-1605.
8. Mark Galassi JD, James Theiler, Brian Gough, Gerard Jungman, Patrick Alken, Michael Booth, Fabrice Rossi (2009) *GNU Scientific Library Reference Manual* (Network Theory Ltd).
9. Jones E, Oliphant T, & Peterson P (2014) SciPy: open source scientific tools for Python.
10. Hunter JD (2007) Matplotlib: A 2D graphics environment. *Computing In Science & Engineering* 9(3):90-95.
11. Ramachandran P & Varoquaux G (2011) Mayavi: 3D visualization of scientific data. *Computing in Science & Engineering* 13(2):40-51.